MOLECULAR AND CELLULAR BIOLOGY, Feb. 2005, p. 1041–1053 Vol. 25, No. 3
0270-7306/05/$08.00+0 doi:10.1128/MCB.25.3.1041–1053.2005

Silencing of Unpaired Chromatin and Histone H2A Ubiquitination in Mammalian Meiosis

Willy M. Baarends,[1]* Evelyne Wassenaar,[1] Roald van der Laan,[2] Jos Hoogerbrugge,[1] Esther Sleddens-Linkels,[1] Jan H. J. Hoeijmakers,[2] Peter de Boer,[3] and J. Anton Grootegoed[1]

Department of Reproduction and Development[1] and MGC-Department of Cell Biology and Genetics,[2] Erasmus MC, University Medical Center, Rotterdam, and Department of Obstetrics and Gynaecology, University Medical Center St. Radboud, Nijmegen,[3] The Netherlands

Received 24 May 2004/Returned for modification 22 July 2004/Accepted 25 October 2004

During meiotic prophase in male mammals, the X and Y chromosomes are incorporated in the XY body. This heterochromatic body is transcriptionally silenced and marked by increased ubiquitination of histone H2A. This led us to investigate the relationship between histone H2A ubiquitination and chromatin silencing in more detail. First, we found that ubiquitinated H2A also marks the silenced X chromosome of the Barr body in female somatic cells. Next, we studied a possible relationship between H2A ubiquitination, chromatin silencing, and unpaired chromatin in meiotic prophase. The mouse models used carry an unpaired autosomal region in male meiosis or unpaired X and Y chromosomes in female meiosis. We show that ubiquitinated histone H2A is associated with transcriptional silencing of large chromatin regions. This silencing in mammalian meiotic prophase cells concerns unpaired chromatin regions and resembles a phenomenon described for the fungus *Neurospora crassa* and named meiotic silencing by unpaired DNA.

Chromatin remodeling is at the basis of control of cell-specific gene expression, cell determination, and differentiation. The nucleosome units of chromatin consist of two each of the histones H2A, H2B, H3, and H4. The N-terminal ends of these core histones extend from the nucleosome and can undergo posttranslational covalent modifications, such as methylation, acetylation, phosphorylation, and ADP-ribosylation of specific amino acid residues. Together, these modifications constitute the so-called histone code (45). Interaction of other nuclear proteins with chromatin is dependent on the histone code at specific chromatin regions and determines local chromatin structure, which can be open or closed. A remarkable component of the histone code is ubiquitination of C-terminal lysine residues of histones H2A and H2B. Ubiquitin, a protein of 7 kDa, can be attached to lysine residues of a specific protein substrate through the action of a multienzyme complex containing ubiquitin-activating (E1), ubiquitin-conjugating (E2), and ubiquitin ligase (E3) enzymes. Polyubiquitination can target proteins for degradation by the proteasome (34, 35). Monoubiquitination of histones, however, is a stable modification that does not decrease the half-life of the target histone (56).

In the yeast *Saccharomyces cerevisiae*, histone H2A ubiquitination is not required for cell growth or sporulation (47), but histone H2B ubiquitination is an essential mechanism involved in sporulation (37). Most importantly, it has been shown that ubiquitination of H2B by the ubiquitin-conjugating enzyme RAD6, interacting with the ubiquitin ligase BRE1, is a prerequisite for dimethylation of histone H3 at lysine residues 4 and 79 (5, 12, 37, 46). This mechanism is thought to be associated with potentiation of gene activation. It is not known whether this "trans-histone" mechanism is conserved between yeast and mammals. RAD6 shows marked evolutionary conservation. The two mammalian homologs of yeast RAD6, Hr6a/Ube2a and Hr6b/Ube2b, both show approximately 70% amino acid sequence identity to yeast RAD6. Previously, we have investigated histone ubiquitination in mice deficient in Hr6b/Ube2B. X-chromosomal *Hr6a*/*Ube2a* and autosomal *Hr6b*/*Ube2b* are functionally equivalent in somatic cells, but gametogenesis requires differential expression or differential functions of the two genes or both (38, 39). *Hr6a* knockout mice show maternal factor infertility (lack of embryo development beyond the two-cell stage), whereas *Hr6b* knockout mice display male infertility (severely impaired spermatogenesis) (38, 39). *Hr6a Hr6b* double-knockout mice are not viable. No defect in H2A ubiquitination was observed in spermatogenic cells of *Hr6b* knockout mice, and the level of H2B ubiquitination was too low to be detected in wild-type and knockout tissues and cells (1).

In mammalian cells, H2A ubiquitination is far more prominent than H2B ubiquitination, and the functional relevance of these modifications in higher organisms remains elusive (56). Marked H2A ubiquitination was observed in meiotic prophase cells, in particular in a specific subnuclear region that contains the heterochromatic X and Y chromosomes (1). This region is called the sex body or XY body, which is formed at the beginning of meiotic prophase, when homologous chromosomes align. This process of chromosome alignment requires development of a protein structure that holds the two chromosomes together, the synaptonemal complex (16). First, axial elements attach to the chromosomal cores, and subsequently the central and transverse elements form the connection. One of the axial element proteins is Sycp3, and immunostaining for this protein is a useful tool to follow progression through meiotic prophase.

* Corresponding author. Mailing address: Department of Reproduction and Development, Erasmus MC, University Medical Center Rotterdam, P.O. Box 1738, 3000 DR Rotterdam, The Netherlands. Phone: 31-104087976. Fax: 31-104089461. E-mail: w.baarends@erasmusmc.nl.

Synaptonemal complex formation coincides with chromosome pairing and synapsis. The heterologous X and Y chromosomes are covered by Sycp3 along their whole length but show synapsis only in short pseudoautosomal regions. From late zygotene onwards, the X and Y chromosomes in the XY body are transcriptionally silent (29).

Localization of ubiquitinated histone H2A (ubi-H2A) to transcriptionally silent XY body chromatin may signify that H2A ubiquitination is linked to transcriptional silencing, also in other chromatin regions and not only in meiotic prophase. The aim of the experiments presented in this paper was to obtain additional information concerning a possible connection between histone H2A ubiquitination and formation or maintenance of silent chromatin regions.

MATERIALS AND METHODS

Isolation of different cell types from mouse testis. For isolation of basic nuclear proteins, a cell preparation containing more than 70% spermatocytes and spermatids was isolated from 30-day-old wild-type FVB/N mice, using a shortened protocol. Iodoacetamide (10 mM) was present throughout the cell isolation procedure to inhibit protein deubiquitination (27), and the isolation procedure was shortened to limit negative effects of iodoacetamide on cell viability, as follows. Decapsulated testes were shaken (90 cycles/min; amplitude, 10 mm) in 20 ml of phosphate-buffered saline (PBS) with Ca^{2+} and Mg^{2+} (137 mM NaCl, 2.7 mM KCl, 1.5 mM KH_2PO_4, 6.5 mM Na_2HPO_4, 1.1 mM $CaCl_2$, 0.5 mM $MgCl_2$), containing 1 mg of trypsin (40 to 110 U/mg; Roche, Mannheim, Germany) per ml, 1 mg of collagenase (0.435 U/mg; Roche) per ml, and 0.5 mg of hyaluronidase (1,000 U/mg; Roche) per ml, in a siliconized 100-ml Erlenmeyer flask at 32 to 34°C for 25 min. The tubule fragments obtained by this enzyme treatment were shaken (120 cycles/min) at 32 to 34°C for 10 min in 20 ml of PBS without Ca^{2+} and Mg^{2+} (137 mM NaCl, 2.7 mM KCl, 1.5 mM KH_2PO_4, 8.1 mM Na_2HPO_4). Larger cell clumps were removed with a Pasteur pipette, and the cell suspension was filtered through a 60-μm-pore-size nylon filter and centrifuged at 250 × *g*.

Isolation of acid soluble nuclear proteins and two-dimensional gel electrophoresis. Nuclei and acid-soluble proteins were isolated from cell preparations as described by Chen et al. (6). The isolated protein fraction was precipitated with 5% (wt/vol) trichloroacetic acid. First-dimension acetic acid-urea-Triton (AUT) gels were run as described by Davie (9) and contained 0.8 M acetic acid, 6 M urea, and 0.375% (vol/vol) Triton X-100. The AUT strips were placed on sodium dodecyl sulfate (SDS)–15% polyacrylamide gels and blotted on nitrocellulose (0.45-μm pore size), using Mini-Protean II electrophoresis and blot cells (Bio-Rad, La Jolla, Calif.). After equilibration of the gel for 30 min in 50 mM acetic acid and 0.5% (wt/vol) SDS, blotting was performed in 25 mM 3-(cyclohexylamino)-1-propanesulfonic acid buffer (pH 10) with 20% (vol/vol) methanol according to the protocol described by Thiriet and Albert (48). ubi-H2A was detected as described by Baarends et al. (1).

Meiotic spread nucleus preparations and immunocytochemistry. Embryonal ovaries were isolated at embryonic day 18 from wild-type, XO, and XY^{tdym1} embryos (generated on a random-bred MF1 background from stocks maintained at the National Institute for Medical Research, London, United Kingdom, and made available by P. Burgoyne, London, United Kingdom). Testes were obtained from 5-week-old wild-type and T(1;13)70H/T(1;13)1Wa (T/T′) mice (Swiss random bred) and from one adult rat (Wistar). Human testicular tissue was obtained as remnant material from a testicular biopsy. Testis and ovary tissues were processed for immunocytochemistry as described by Peters et al. (33). Spread nuclei of spermatocytes and oocytes were double or triple stained with rabbit polyclonal or mouse monoclonal anti-Sycp3 (a gift from C. Heyting, Wageningen, The Netherlands), mouse monoclonal immunoglobulin M (IgM) anti-ubi-H2A (Upstate, Waltham, Mass.), mouse monoclonal anti-RNA polymerase II (the 8wg16 detects total RNA polymerase II) (Abcam, Cambridge, United Kingdom), mouse monoclonal anti-trimethylated H3 lysine 27 (Abcam), rabbit polyclonal anti-$Rad18^{Sc}$ (as described by van der Laan et al. [53]), rabbit polyclonal antiubiquitin (DakoCytomation, Glostrup, Denmark), rabbit polyclonal anti-trimethylated H3 lysine 9 (Upstate), rabbit polyclonal anti-Hr6a/b (1:100) (described by van der Laan et al. [53]), and rabbit polyclonal anti-γ-H2AX (Upstate). For polyclonal primary antibodies, the secondary antibodies were fluorescein isothiocyanate (Sigma, St. Louis, Mo.), tetramethyl rhodamine isocyanate (TRITC) (Sigma), or Alexa 350 (Molecular Probes, Eugene, Oreg.)-labeled goat anti-rabbit IgG antibodies; FITC-, TRITC-, or Alexa 350-labeled goat anti-mouse IgG and FITC-labeled goat anti-mouse IgM (Sigma) were used as secondary antibodies for monoclonal anti-Sycp3 (IgG), anti-RNA polymerase II (IgG), anti-trimethylated H3 lysine 27, and anti-ubi-H2A (IgM). To perform double immunolabelings with mouse monoclonal anti-ubi-H2A IgM and mouse monoclonal anti-trimethylated H3 lysine 27, cells were first immunostained with anti-ubi-H2A, followed by immunostaining with anti-trimethylated H3 lysine 27. Negative controls were included to verify that the secondary IgG antibody did not cross-react with remaining anti-ubi-H2A IgM from the first round of immunocytochemistry. Before incubation with antibodies, slides were washed in PBS (three times for 10 min each), and nonspecific sites were blocked with 0.5% (wt/vol) bovine serum albumin (BSA) and 0.5% (wt/vol) milk powder in PBS. Primary antibodies were diluted in 10% (wt/vol) BSA in PBS, and incubations were overnight at room temperature in a humid chamber. Subsequently, slides were washed (three times for 10 min each) in PBS, blocked in 10% (vol/vol) normal goat serum (Sigma) in blocking buffer (supernatant of 5% [wt/vol] milk powder in PBS centrifuged at 20,800 × *g* for 10 min), and incubated with secondary antibodies in 10% normal goat serum in blocking buffer at room temperature for 2 h. Finally, the slides were washed (three times for 10 min each) in PBS (in the dark) and embedded in Vectashield containing DAPI (4′,6′-diamidino-2-phenylindole) (Vector Laboratories, Burlingame, Calif.) to counterstain the DNA. When Alexa 350-labeled second antibody was present on the slides, Vectashield without DAPI was used. Fluorescent images from spread nuclei were observed with a fluorescence microscope (Axioplan 2; Carl Zeiss, Jena, Germany) equipped with a digital camera (Coolsnap-pro; Photometrics, Waterloo, Canada). Digital images were processed with Photoshop software (Adobe Systems).

FISH. Following immunocytochemistry, the positions of selected nuclei on the slide were determined, and fluorescent in situ hybridization (FISH) with STAR*FISH mouse whole-chromosome-specific paints (1200XmCy3 and 1200YmCy3; Cambio, Cambridge, United Kingdom) was performed according to the manufacturer's protocol to detect the X or Y chromosomes. All fluorescent signal obtained after immunocytochemistry had disappeared after FISH. To make sure that remaining signal from immunocytochemistry is not mistaken for a FISH signal, the color of the fluorescent dye for FISH differs from the color of the fluorescent dye coupled to the second antibody that was used to visualize ubi-H2A or $Rad18^{Sc}$. If a specific signal was not obtained, the procedure was performed a second time, and this always resulted in a positive signal in the majority of nuclei. The specificity of hybridization was confirmed by using male meiotic spread nucleus preparations; a positive signal colocalized with the XY body of pachytene spermatocytes (not shown). Since the X and Y chromosome probes are labeled with the same fluorescent dye and both probes were used on the same slide in subsequent experiments (first the X chromosome probe and then the Y chromosome probe), some X-chromosomal signal remains visible after the second FISH with the Y-chromosomal probe.

To localize telomeres, a TRITC-labeled peptide nucleic acid probe directed against mouse telomeres (a gift from M. Zijlmans, Rotterdam, The Netherlands) was used to identify telomeres in spread nuclei of spermatocytes. Meiotic spread nucleus preparations were denatured in 70% (vol/vol) deionized formamide in 2× SSC at 72°C for 2.5 min, followed by dehydration with ethanol. Slides were air dried, and 20 μl of denatured probe (0.3 μg/ml) in hybridization mix (70% [vol/vol] deionized formamide, 10 mM Tris-HCl [pH 7.0], 0.25% [wt/vol] blocking reagent [DuPont/NEN, Boston, Mass.; stock of 1% {wt/vol} in 40 mM Tris-HCl {pH 7.0}]) was applied. Hybridization was carried out under a coverslip in a humid chamber for 2 h in the dark at room temperature, followed by sequential washing in 70% (vol/vol) formamide–10 mM Tris-HCl (pH 7.0)–0.1% (wt/vol) BSA (twice for 15 min each) and 0.1 M Tris-HCl (pH 7.0)–0.15 M NaCl–0.08% (vol/vol) Tween 20 (three times for 5 min each). Subsequently, immunocytochemistry with the anti-ubi-H2A monoclonal antibody was carried out as described above. Digital images were obtained and processed as described above. FISH images were combined with immunocytochemical images by using Adobe Photoshop software, and alignment was obtained by alignment of nonspecific signals present in both images. In addition, in some cases, the red fluorescent FISH signal was converted to white to obtain better contrast.

Immunohistochemistry. Kidney and liver tissues were isolated from male and female adult rats (Wistar), fixed in phosphate-buffered formalin (30 mM NaH_2PO_4, 45 mM Na_2HPO_4, 4% [vol/vol] formaldehyde [pH 6.8]) for 6 to 18 h at 4°C, dehydrated, and embedded in paraffin. Sections of 8 μm were collected on 3-aminopropyltriethoxysilane (Sigma)-coated slides and dried overnight. After deparaffinization, endogenous peroxidase was blocked by incubation in 3% (vol/vol) H_2O_2 for 20 min, followed by a rinse with tap water. The slides were then incubated for 20 min in a microwave oven at 1,000 W in 0.01 M citric acid, pH 6.0. The slides were allowed to cool and washed with distilled water and PBS.

The slides were blocked for 20 min in PBS with 0.5% (wt/vol) BSA and 0.5% (wt/vol) nonfat milk and incubated with anti-ubi-H2A (diluted 1:10 in 10% BSA in PBS) overnight at room temperature. Subsequently, the slides were washed in PBS and incubated for 1 h at room temperature with the second antibody (biotinylated goat anti-mouse antibody; DAKO, Glostrup, Denmark), which was diluted 1:200 in PBS containing 2% (vol/vol) normal goat serum. The antibody-antigen complexes were detected by incubation for 30 min with avidin-biotin complex reagent (DAKO) according to the protocol supplied by the manufacturer, followed by staining with 3,3′-diaminobenzidine tetrahydrochloride metal concentrate (Pierce, Rockford, Ill.), counterstaining with hematoxylin, and mounting.

RESULTS

ubi-H2A is present in the XY bodies of mouse, rat, and human. The monoclonal anti-ubi-H2A IgM antibody binds ubiquitinated H2A on one-dimensional SDS-polyacrylamide gels (1, 54). To verify specificity, we performed Western blot analyses (Fig. 1A). Anti-ubi-H2A recognized one clear spot, corresponding to the expected localization of ubi-H2A, and no signal corresponding to ubi-H2B was detected.

In meiotic spread nuclei, the degree of synapsis of homologous chromosomes can be determined with an antibody that recognizes Sycp3, a component of the axial and lateral elements of the synaptonemal complex (22). Using this marker, the leptotene, zygotene, pachytene, and diplotene stages of meiotic prophase can be detected. At pachytene, all autosomal bivalents have fully synapsed, and the XY body has become a prominent structure. The spread nuclei are prepared in such a way that only chromatin-associated proteins are maintained, and ubi-H2A shows marked localization to the XY body (Fig. 1B). In addition, nuclear foci with lower signal intensity are observed in late pachytene and early diplotene nuclei, and a significant fraction of these foci colocalize with (near) telomeric regions (Fig. 1B [insets] and C). As a control for specificity of the antibody on meiotic spread nuclei of spermatocytes, we looked at colocalization between antiubiquitin and anti-ubi-H2A. In accordance with the presence of ubi-H2A in the XY body, there was intense staining of ubiquitin in the XY body and a lower overall staining of the nucleus, most likely due to the presence of other ubiquitinated proteins (Fig. 1B and C). ubi-H2A also marked the XY bodies of rat and human spermatocytes (Fig. 1D), indicating that H2A ubiquitination is an evolutionarily conserved feature of XY body chromatin.

ubi-H2A marks the Barr body in female somatic cells. The XY body is transcriptionally silent, and the present results suggest that ubiquitinated H2A could be a general feature of inactive chromatin domains. In female somatic cells, one of the two X chromosomes becomes inactivated to accomplish dosage compensation. In 1949 the inactive X chromosome in female somatic cells was recognized for the first time and named the Barr body (3). We studied the accumulation of ubi-H2A in male and female somatic cells to determine whether ubi-H2A localized to the Barr body. Immunohistochemical staining of kidney sections from adult male and female rats revealed a marked nuclear spot of ubi-H2A accumulation only in female cells (Fig. 2A). In addition, in female liver cells, which contain many polyploid cells, we often observed two spots (Fig. 2B). Also, in spread nucleus preparations of XO, XY (sex reversed), and XX female fetal ovaries (see experiments described below), we observed a single ubi-H2A spot exclusively in pregranulosa cells from fetal XX ovaries (Fig. 2C). To verify that this ubi-H2A spot in XX cells marks the Barr body, we performed a sequential double immunocytochemical staining of XX fetal ovary cells with anti-ubi-H2A, followed by anti-trimethylated H3 lysine 27, a known marker of the inactivated X chromosome during female embryogenesis (36, 41). All ubi-H2A spots colocalized with trimethylated H3 lysine 27 signal (Fig. 2D); some nuclei contained only trimethylated H3 lysine 27 at the inactive X chromosome, and not all nuclei stained positive (not shown).

ubi-H2A localizes to unpaired and silenced chromatin regions in male meiotic prophase. To study the relationship between accumulation of ubi-H2A, silencing of DNA during meiotic prophase, and homologous chromosome pairing, we studied a male mouse model that carries two different but nearly identical translocations between chromosomes 1 and 13, named T(1;13)70H/T(1;13)1Wa (abbreviated T/T′). A small difference in the location of the translocation breakpoints causes the two 1^{13} and 13^{1} homologs to be not fully identical, and this leads to a pairing problem during meiotic prophase (11, 32). The degree of synapsis that is achieved varies among nuclei and also between animals. The percentage of spermatocyte nuclei with complete synapsis of all bivalents positively correlates with fertility. In particular, the small 1^{13} bivalent often remains only partially synapsed. To study ubi-H2A localization on the small translocation bivalent in pachytene spermatocyte nuclei, we selected nuclei that showed normal morphology of the synaptonemal complex and accumulation of ubi-H2A in the XY body. The morphology of the 1^{13} bivalent was classified as partially synapsed rest (PR) (low degree of synapsis), partially synapsed A shape (PA) (intermediate degree of synapsis), partially synapsed horsheshoe shape (PH) (near-complete synapsis), or completely synapsed (CS). On incompletely synapsed PR/PA bivalents, we found ubi-H2A accumulation in 19 out of 26 nuclei, whereas for the PH/CS bivalents only 6 out of 30 nuclei showed accumulation of ubi-H2A. Overall, the fraction of nuclei with ubi-H2A-positive 1^{13} bivalents decreased with an increasing degree of (heterologous) synapsis (Fig. 3).

RNA polymerase II immunolocalization was used as a marker for transcriptionally active chromatin. The signal-to-noise ratio for this antibody is optimal in late pachytene and early diplotene cells. Analysis of the RNA polymerase II signal covering the 1^{13} translocation bivalent in spermatocyte nuclei from the T/T′ mice revealed a positive correlation between fluorescent signal and degree of 1^{13} synapsis. Of 23 nuclei analyzed, three 1^{13} translocation bivalents showed complete synapsis (CS configuration), associated with a high level of RNA polymerase II immunoexpression on chromatin covering the 1^{13} bivalent. This was also observed for one out of nine nuclei with near-complete synapsis (PH configuration). The rest of the partially synapsed 1^{13} translocation bivalents (PH, PA, and PR) showed no (11 nuclei) or a low level of (8 nuclei) RNA polymerase II immunoexpression. This indicates that the incompletely synapsed 1^{13} bivalent is at least partially transcriptionally silenced (Fig. 4A).

In *S. cerevisiae*, histone H2A ubiquitination is not detected (47). H2B ubiquitination is functionally linked to histone H3 lysine 4 dimethylation (5). This so-called trans-histone regulatory pathway is thought to be associated with transcription activation (5, 8). In contrast, H2A ubiquitination in higher

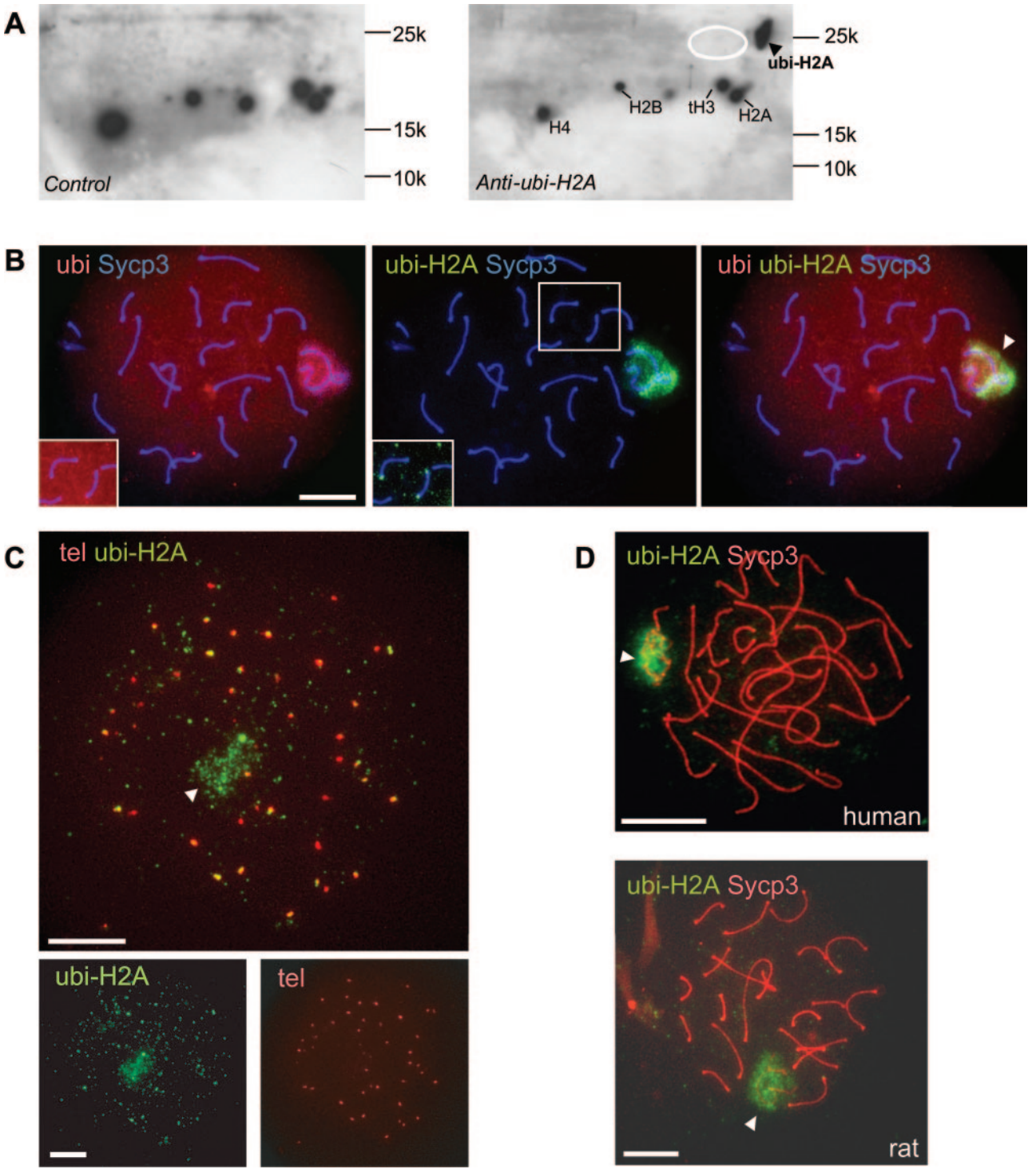

FIG. 1. ubi-H2A marks the XY bodies and telomeres of pachytene spermatocytes. A: Western blots of basic nuclear proteins separated on two-dimensional AUT-SDS-polyacrylamide gels (first dimension, AUT; second dimension, SDS) were stained with anti-ubi-H2A (right panel) or with second antibody only (control, left panel). A specific signal is detected at the expected position for ubi-H2A (arrowhead). The approximate positions of histones H2A, H2B, tH3, and H4 are indicated for reference. Positions and molecular weights of marker proteins are indicated. The expected approximate position of ubi-H2B is indicated by the white ellipse, and the blots are overexposed to show that no ubi-H2B is detected. B: Spermatocyte spread nuclei from wild-type mice stained with a mouse monoclonal IgG antibody against Sycp3 (blue), a rabbit polyclonal antiubiquitin antibody (red), and a mouse monoclonal IgM antibody against ubi-H2A (green). Both ubi and ubi-H2A mark XY body chromatin (arrowhead in right panel, showing the merged signals). Anti-ubi also detects other ubiquitinated proteins associated with chromatin in the rest of the nucleus. Upon overexposure, ubi and ubi-H2A are detected at the ends of some synaptonemal complex axes (insets). C: FISH analysis of telomeres (tel) (red) followed by immunocytochemistry with anti-ubi-H2A (green) of an early diplotene cell. Diplotene is identified by the presence of a low level of ubi-H2A in the XY body (arrowhead) and the high number of telomeric foci (more than 40, with double foci still attached counted as one) and splitting of telomeres. The upper panel shows that around 30 telomere foci colocalize, at least partially, with ubi-H2A. A total of approximately 100 ubi-H2A foci are observed outside the XY body area, indicating that chromatin regions other than the XY body and (near) telomeric regions also accumulate ubi-H2A. The bottom panels show lower-magnification images of the single fluorescent signals. D: Spermatocyte spread nuclei from rat and human stained with anti-Sycp3 (red) and anti-ubi-H2A (green). ubi-H2A marks XY body chromatin (arrowhead) in both species. Bars, 20 μm.

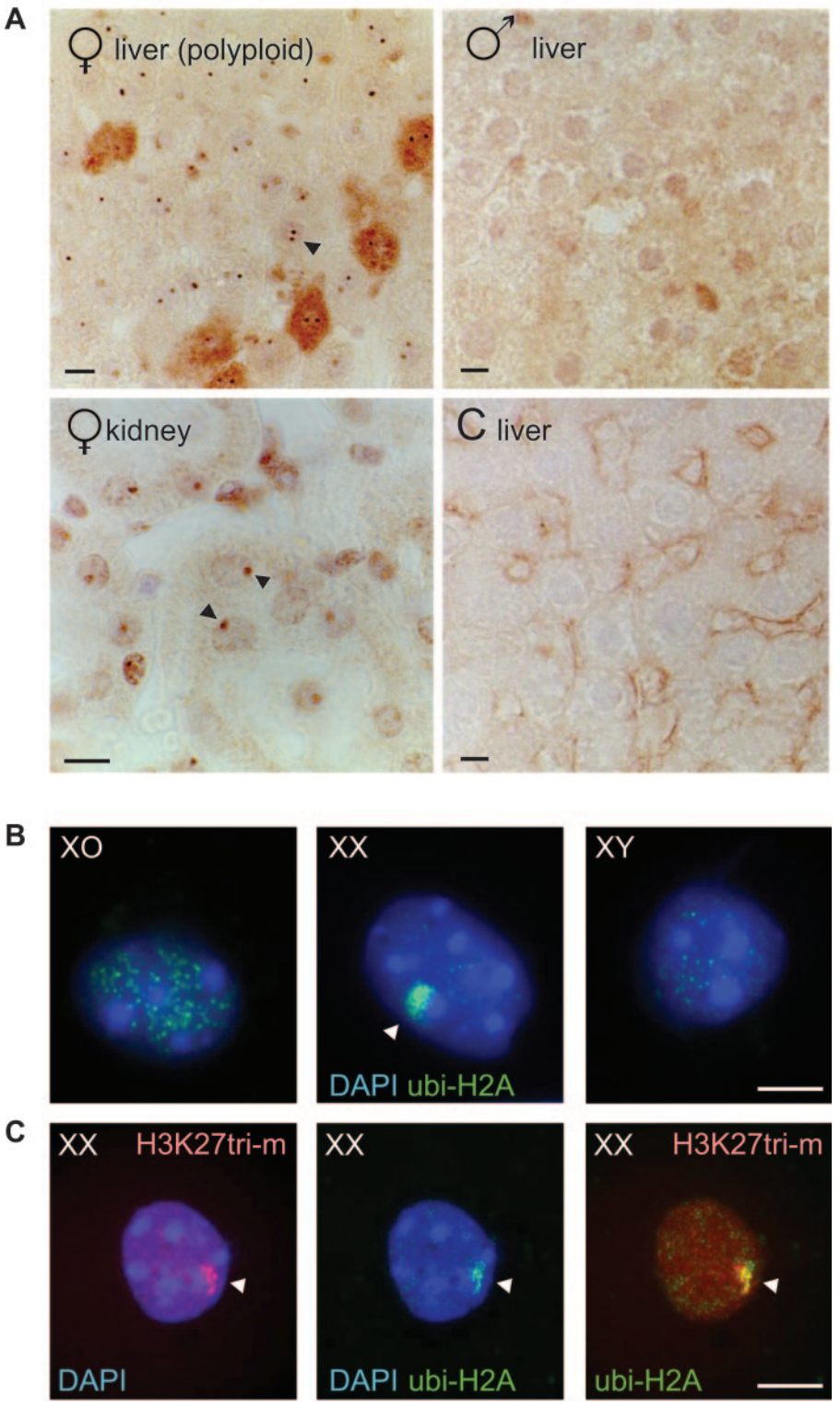

FIG. 2. ubi-H2A marks the inactive X chromosome (Barr body) in female somatic cells. A: Immunohistochemical analysis of ubi-H2A localization in rat female liver and kidney sections and in male liver sections. Control (C liver): incubation without first antibody. In female kidney nuclei, high-level accumulation of ubi-H2A is seen as a single nuclear spot (arrowhead). In addition, two spots are often observed in polyploid female liver nuclei (arrowhead). These spots are not observed in male tissues. Bars, 10 μm. B: Immunocytochemical detection of ubi-H2A in XO, XX, and XY^{tdym1} pregranulosa cells. A variable number of small foci, of unknown nature, is present in all nuclei, but only the XX pregranulosa cells accumulate ubi-H2A in a single large spot in the periphery of the nucleus (arrowhead). Bar, 20 μm. C: Immunocytochemical detection of H3 lysine 27 trimethylation (H3K27tri-m) (red) and ubi-H2A (green) in XX pregranulosa cells. H3 lysine 27 methylation and ubi-H2A largely colocalize in a single large spot in the periphery of the nucleus (arrowhead). Bar, 20 μm.

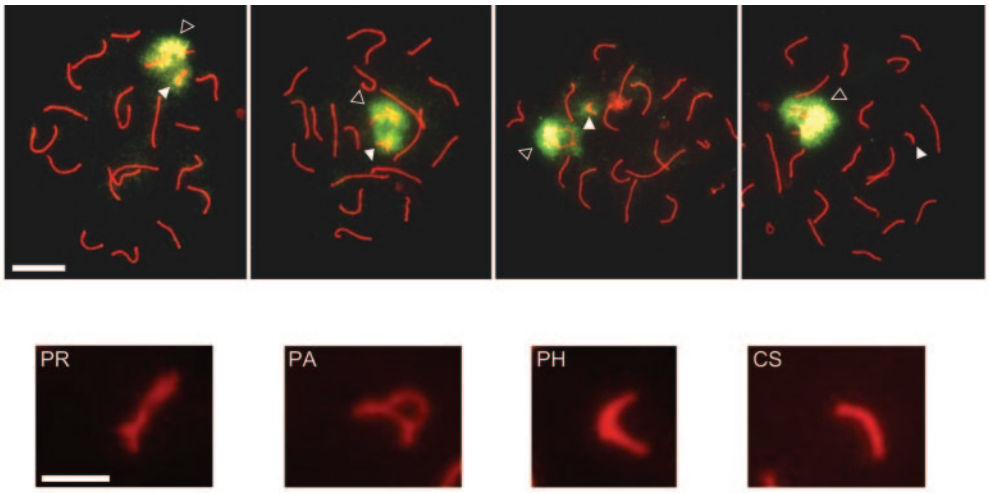

ubi-H2A	#PR	#PA	#PH	#CS	Tot
-	1	2	7	12	22
+/-	2	2	1	4	9
+	9	10	4	2	25
Tot	12	14	12	18	56

FIG. 3. ubi-H2A marks the partially synapsed 1^{13} translocation bivalent of T/T′ spermatocytes. The top row shows four T/T′ pachytene spermatocyte spread nuclei stained with anti-ubi-H2A (green) and anti-Sycp3 (red). The closed arrowheads indicate the location of the 1^{13} bivalent, at different positions with respect to the XY body (open arrowheads). Bar, 20 μm. The images in the second row represent the four defined groups of 1^{13} synapsis morphologies, detected with anti-Sycp3 staining and shown at a higher magnification (bar, 5 μm). PR, partially synapsed rest; PA, partially synapsed A shape; PH, partially synapsed horseshoe shape; CS, complete synapsis. The table shows that an increasing fraction of 1^{13} bivalents is ubi-H2A negative when synapsis is more complete. Absolute numbers of scored nuclei with no ubi-H2A signal (−), a low ubi-H2A signal (+/−), or a clear ubi-H2A signal (+) are indicated. Tot, total number of nuclei counted.

eukaryotes may be associated with transcriptional silencing. H2A ubiquitination might be functionally coupled to methylation of other H3 lysines that mediate silencing, in analogy to the link between H2B ubiquitination, H3 lysine 4 dimethylation, and transcription activation. In accordance with the silent chromatin configuration of the XY body, we found that the XY body was covered by a relatively low level of H3 lysine 4 dimethylation (not shown). Trimethylation of H3 lysine 9 is a known marker of pericentromeric heterochromatin in mammals (31). This prompted us to investigate a possible association between H3 lysine 9 trimethylation and H2A ubiquitination in spermatocytes. Triple immunostaining of T/T′ spermatocyte nuclei with anti-Sycp3, anti-ubi-H2A, and anti-trimethylated H3 lysine 9 revealed that a functional link between these two modifications is unlikely. Figure 4B and C show that pericentromeric DNA in spermatocytes is marked by increased trimethylation of H3 lysine 9 but not by ubi-H2A. Furthermore, a relatively low level of H3 lysine 9 trimethylation marked the XY body and the unsynapsed 1^{13} bivalent, but only transiently (Fig. 4B). XY-associated trimethylation of H3 lysine 9 preceded H2A ubiquitination and had disappeared from the XY bodies of late pachytene nuclei in which ubi-H2A is still present (Fig. 4C). Since the initiation of somatic X inactivation is accompanied by increased trimethylation of H3 lysine 27, we also investigated a possible link between this modification and H2A ubiquitination in T/T′ spermatocytes. We found that the XY body as well as the 1^{13} bivalent showed a relatively low level of H3 lysine 27 trimethylation (Fig. 4D).

Another marker of transcriptionally silenced unsynapsed chromatin regions during meiosis is phosphorylated histone H2AX (γ-H2AX). This modification occurs in response to DNA double-strand breaks in somatic cells and is also associ-

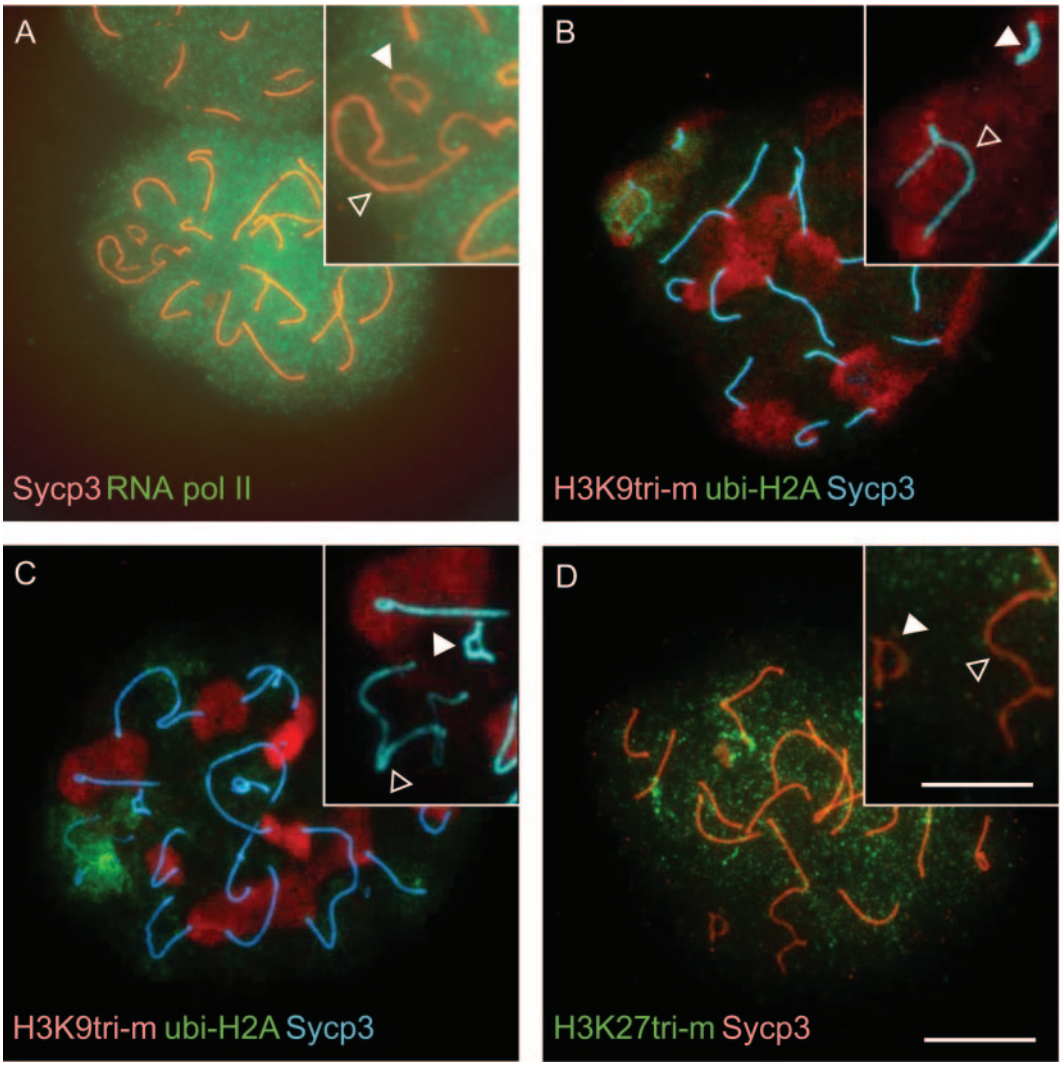

FIG. 4. Ubiquitination of H2A is not associated with increased trimethylation of histone 3 at lysine 9 or lysine 27. A: Double immunostaining of a T/T′ pachytene spermatocyte spread nucleus with anti-Sycp3 (red) and anti-RNA polymerase (pol) II (green). The inset shows a larger magnification of the area containing the XY body (open arrowhead) and the 1^{13} bivalent (closed arrowhead). B: Triple immunostaining of a T/T′ pachytene spermatocyte spread nucleus with anti-trimethylated H3 lysine 9 (H3K9tri-m) (red), anti-ubi-H2A (green), and anti-Sycp3 (blue). The inset shows double staining of anti-trimethylated H3 lysine 9 and anti-Sycp3 in the area containing the XY body (open arrowhead) and the 1^{13} bivalent (closed arrowhead). Both the translocation bivalent (PH group) and the XY body accumulate trimethylated H3 lysine 9 and ubi-H2A. The level of ubi-H2A appears to be higher in areas that contain a somewhat lower trimethylated H3 lysine 9 signal. C: As in panel B, but this late pachytene spermatocyte shows no accumulation of trimethylated H3 lysine 9 in the area containing the XY body and the 1^{13} bivalent (PA group). D: As in panel A, but this spread nucleus was incubated with anti-trimethylated H3 lysine 27 (H3K27tri-m) (green) and anti-Sycp3 (red). H3 lysine 27 trimethylation is relatively low in the area that covers the XY body and the 1^{13} bivalent (PR group). Bar, 20 μm; bar in inset, 10 μm.

ated with meiotic double-strand breaks (25, 40). Furthermore, it has been shown that accumulation of γ-H2AX on the X and Y chromosomes during late zygoytene in mouse spermatocytes is a prerequisite for XY body formation (13). Previously, it had been shown that γ-H2AX also accumulates on the partially synapsed 1^{13} bivalent in T/T′ mice (25). Triple immunostainings of meiotic nuclei from T/T′ mice with anti-γ-H2AX, anti-ubi-H2A, and anti-Sycp3 revealed that 1^{13} bivalents that accumulated ubi-H2A also showed increased γ-H2AX staining (Fig. 5A). However, γ-H2AX accumulation on XY body chromatin as well as on chromatin of the 1^{13} bivalent was often observed in the absence of ubi-H2A (Fig. 5B). This may be due to the fact that γ-H2AX accumulates earlier during meiotic prophase and persists longer than ubi-H2A.

In *S. cerevisiae*, the E2 enzyme RAD6 and the E3 enzyme RAD18 are key factors in a mechanism that tolerates the presence of DNA damage during DNA replication. In this so-called replicative damage bypass mechanism (23, 51), RAD6 interacts with RAD18 (2). Replicative damage bypass does not require histone H2B ubiquitination (37). We have identified the mouse *Rad18*^{Sc} gene, and mRNA expression from this gene was shown to be highly elevated in mouse testis, in particular in primary spermatocytes in meiotic prophase (52). The Rad18^{Sc} protein was found in a relatively high con-

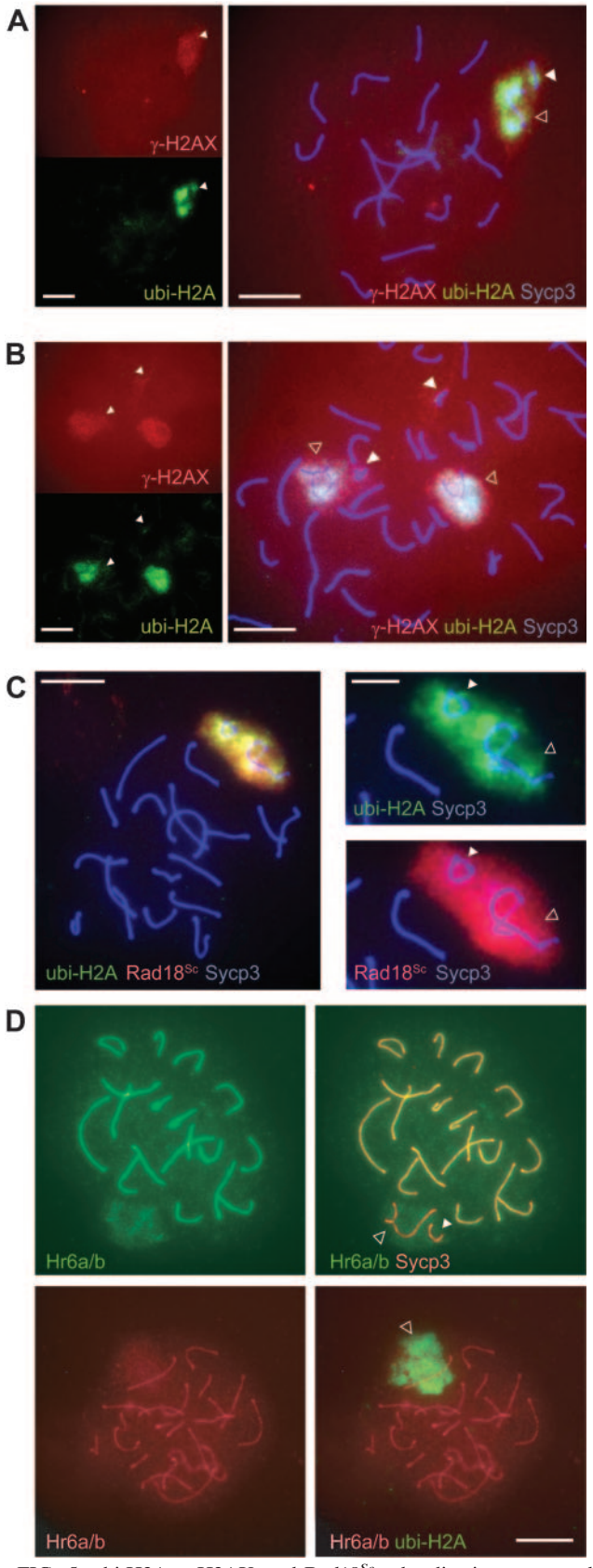

FIG. 5. ubi-H2A, γ-H2AX, and Rad18^{Sc} colocalize in unsynapsed chromatin regions of late pachytene spermatocytes. A: Triple immunostaining of a T/T′ pachytene spermatocyte spread nucleus with anti-γ-H2AX (red), anti-ubi-H2A (green), and anti-Sycp3 (blue). The left panel shows single immunostaining (lower magnification), and the right panel shows triple immunostaining (higher magnification). Both γ-H2AX and ubi-H2A accumulate on the partially synapsed 1^{13} bivalent (PR group). B: As in panel A, but two spread nuclei that accumulate γ-H2AX but not ubi-H2A on partially synapsed 1^{13} bivalents (PA and PH group) are shown. C: The left panel shows triple immunostaining of a T/T′ pachytene spermatocyte spread nucleus with anti-Sycp3 (blue), anti-Rad18^{Sc} (red), and anti-ubi-H2A (green). Bar, 20 μm. The right panels show a higher magnification (bar, 10 μm) of the ubi-H2A/Sycp3 and the Rad18^{Sc}/Sycp3 double staining of an XY body (open arrowhead) and a PA group 1^{13} bivalent (closed arrowhead). D: The upper two panels show a T/T′ spermatocyte spread nucleus immunostained with anti-Hr6a/b (green) and anti-Sycp3 (red). A diffuse Hr6a/b signal covers the XY body (open arrowhead) and the 1^{13} bivalent (closed arrowhead). The highest Hr6a/b signal is observed on synapsed synaptonemal complex. The lower two panels show a T/T′ spermatocyte spread nucleus immunostained with anti-Hr6a/b (red) and anti-ubi-H2A (green). The diffuse Hr6a/b signal (most likely covering the XY body and the 1^{13} bivalent [open arrowhead]) colocalizes with ubi-H2A. Bar, 20 μm.

centration in the XY bodies of these primary spermatocytes at several subsequent steps of meiotic prophase (53). In addition, the ubiquitin ligase Rad18^{Sc} also localizes to the unsynapsed 1^{13} bivalent in pachytene spermatocytes of T/T′ mice (53). Triple immunostaining with anti-ubi-H2A, anti-Rad18^{Sc}, and anti-Sycp3 revealed colocalization of Rad18^{Sc} and ubi-H2A on the XY body and on the partially synapsed translocation bivalents in most nuclei (Fig. 5C). It appears that during male meiotic prophase, Rad18^{Sc} accumulation, similar to that of γ-H2AX, precedes that of ubi-H2A, and Rad18^{Sc} also remains present in early diplotene nuclei when ubi-H2A staining has disappeared. Overall, the immunofluorescent Rad18^{Sc} signal is more intense than that of ubi-H2A. Therefore, the lack of colocalization of Rad18^{Sc} and ubi-H2A in some nuclei is most likely due to differences in the timing and level of accumulation of the two proteins. Hr6a and Hr6b appear to be less tightly bound to chromatin than Rad18^{Sc}, because we have observed that the protein is partially lost from spread nucleus preparations as determined with an antibody that recognizes both RAD6 homologs (anti-Hr6a/b) (53). In fixed spermatocytes, Hr6a/b is present throughout the nucleus, including the XY body (53). We investigated colocalization of Hr6a/b with ubi-H2A in spread nucleus preparations; the spread nuclei allow identification of the 1^{13} bivalent and also provide access to the anti-IgM antibody required for ubi-H2A localization. We found that in such spread nucleus preparations of pachytene T/T′ spermatocytes, Hr6a/b is preferentially retained on synapsed synaptonemal complex axes and shows a more diffuse staining of the chromatin surrounding the unsynapsed XY and 1^{13} bivalent during midpachytene (Fig. 5D). This diffuse chromatin staining increases concomitantly with an increase of the ubi-H2A signal.

ubi-H2A accumulates on unsynapsed chromosomal regions in XY and XO oocytes. In XO females, the single X chromosome remains unpaired during meiotic prophase. In XY^{tdym1} mice, the sex-determining gene *Sry* is deleted, and therefore all of these animals develop as females (24). In meiotic prophase in embryonic ovaries of XY^{tdym1} mice, the X and Y chromosomes pair in approximately 19% of the cells, but no XY body-like structure has been observed (49). In pachytene oo-

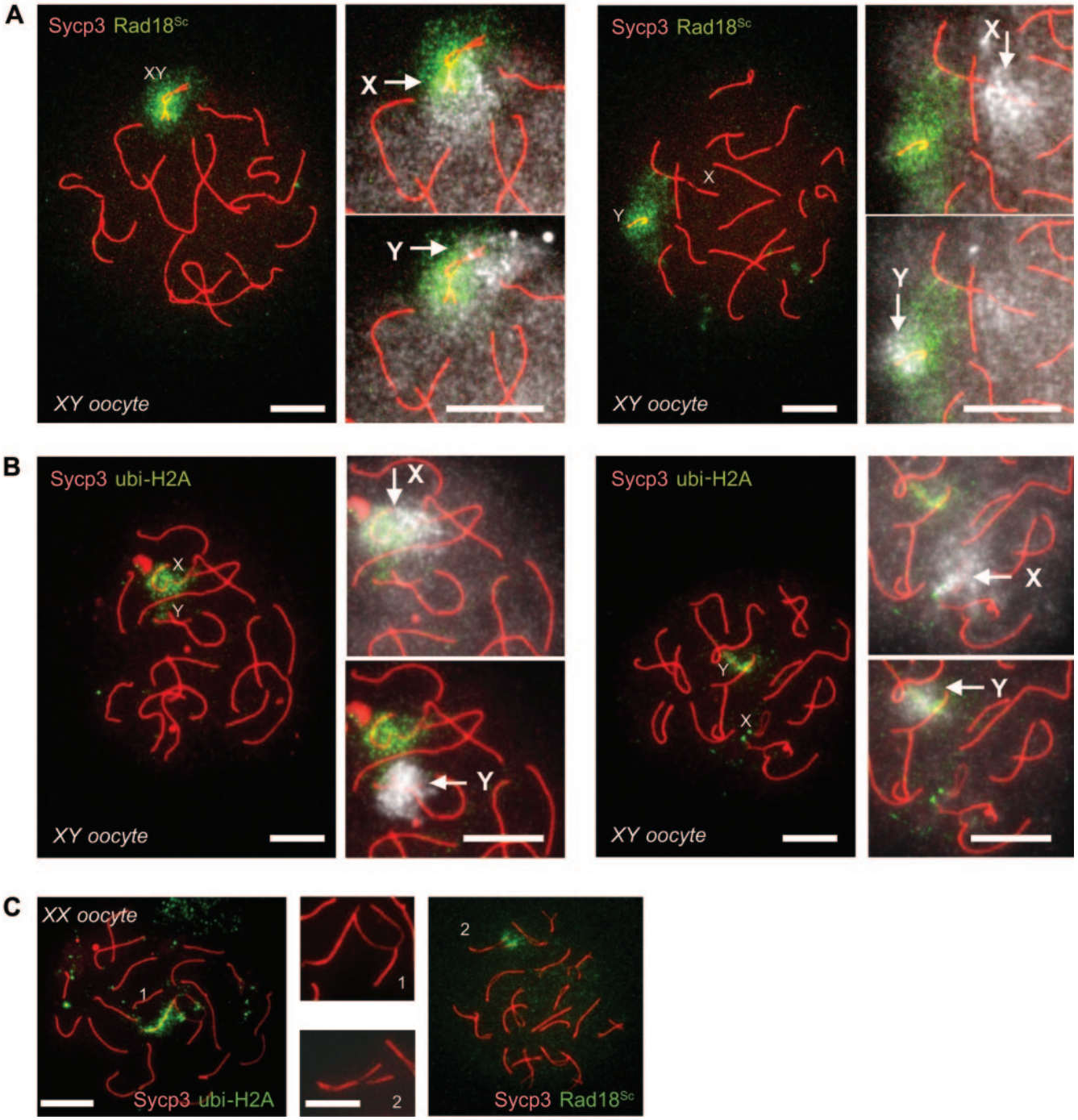

FIG. 6. ubi-H2A and Rad18^{Sc} mark unsynapsed chromosome regions in oocytes. A: Two XY oocyte spread nuclei immunostained with anti-Rad18^{Sc} (green) and anti-Sycp3 (red). The locations of the X and Y chromosomes are indicated. The smaller panels to the right of each nucleus show enlargements of the X and Y chromosomal areas with the white FISH signals for either X or Y (arrows). In the nucleus shown on the left, X and Y are partially synapsed and Rad18^{Sc} accumulates mainly on X-chromosomal chromatin. In the nucleus shown on the right, X and Y have separated, and Rad18^{Sc} accumulation is observed only on the Y chromosome. In this nucleus, the X-chromosomal Sycp3 axis is short and thick, indicating self-synapsis. Note that some X FISH signal is still visible after Y FISH (see Materials and Methods). B: Two XY oocyte spread nuclei immunostained with anti-ubi-H2A (green) and anti-Sycp3 (red). The smaller panels to the right of each nucleus show enlargements of the X and Y chromosomal areas with the white FISH signals for either X or Y (arrows). In both nuclei, X and Y have separated, but ubi-H2A marks the X chromosome in the nucleus in the left panel (the Y chromosome appears to undergo heterologous synapsis) and the Y chromosome in the nucleus in the right panel (the X chromosome appears to be unsynapsed). C: XX oocyte spread nucleus immunostained with anti-Sycp3 (red) and either anti-ubi-H2A (left panel) or anti-Rad18^{Sc} (right panel) (green). The two images in the middle show enlargements (bar, 10 μm) of the aberrant synaptonemal complex morphology (Sycp3 staining) in the respective ubi-H2A (1)- and Rad18^{Sc} (2)-positive regions. Bars, 20 μm unless otherwise indicated.

TABLE 1. Immunoexpression of ubi-H2A, Rad18^{Sc}, and γ-H2AX in XO and XY pachytene oocytes

Protein	No. (%) of nuclei with a single positive staining area[a]	
	XO	XY
ubi-H2A	37 (18.5)	73 (36.5)
Rad18^{Sc}	104 (52)	119 (59.5)
γ-H2AX	93 (46.5)	140 (70)

[a] Two hundred nuclei were counted for each antibody and genotype.

cytes from these XO and XY^{tdym1} mice, we found accumulation of ubi-H2A and Rad18^{Sc} in a single subnuclear region in a large fraction of cells (Fig. 6A and B; Table 1). FISH analysis was used to detect the X and Y chromosomes. For Rad18^{Sc} and ubi-H2A, immunoexpression colocalized with the X chromosome signal in approximately 50% of XY pachytene oocyte nuclei ($n = 14$ for each antibody). In the same two groups of nuclei, the univalent Y chromosome signal colocalized with immunoexpression of Rad18^{Sc} and ubi-H2A when Rad18^{Sc} and ubi-H2A were absent from the X chromosome. In XO oocytes, Rad18^{Sc} immunoexpression, when present, colocalized with the X chromosome FISH signal (not shown). In some nuclei, the X and Y chromosomes are partially synapsed. In this situation, immunoexpression covered both sex chromosomes or mainly localized to the X chromosome (Fig. 6A). In one nucleus with X and Y clearly separated, we observed accumulation of ubi-H2A on both sex chromosomes (not shown). The absence of Rad18^{Sc} or ubi-H2A from sex chromosomes appeared to correlate with heterologous synapsis or self-synapsis (Fig. 6A, right panel, and B, left panel). A minority of nuclei with unsynapsed sequences showed an absence of Rad18^{Sc} or ubi-H2A accumulation (Fig. 6B, right panel). Local accumulation of Rad18^{Sc} and ubi-H2A is rarely detected in XX oocytes. If present, the signal covers chromatin that shows aberrant synaptonemal complex patterns indicating partial synapsis (Fig. 6C). Double immunostaining of XO and XY oocytes with anti-ubi-H2A and anti-Rad18^{Sc} showed the Rad18^{Sc} signal in a larger percentage of the nuclei (Table 1), but ubi-H2A always colocalized with Rad18^{Sc}.

Incomplete chromosome synapsis leads to transcriptional silencing in oocytes. Similar to the observed silencing of unpaired chromatin regions in T/T′ spermatocytes, we found that immunoexpression of RNA polymerase II in XO and XY oocytes was frequently lower in an area covering the single X or Y chromosome or both, as determined by the presence of thinner synaptonemal complex axes (Fig. 7A). In addition, coimmunostaining of anti-Rad18^{Sc} and anti-RNA polymerase II of XO and XY oocytes revealed that areas with lower RNA polymerase II immunoexpression colocalized with regions of intense Rad18^{Sc} signal (Fig. 7B). In accordance with these data, colocalization of ubi-H2A with γ-H2AX was observed (Fig. 7C). Based on γ-H2AX accumulation as a marker for transcriptional silencing, it appears that the X or Y chromosome or both chromosomes do not undergo silencing in all pachytene XY oocytes (Table 1).

DISCUSSION

Histone H2A and H2B ubiquitination. Ubiquitination of H2B in yeast is involved in gene activation, as it takes part in trans-histone control of trimethylation of H3 at lysines 4 and 79 (5, 8). Paradoxically, H2B ubiquitination is also required for gene silencing. It has been suggested that inhibition of H2B ubiquitination leads to reduced formation of active chromatin and loss of silencing proteins from regions that are normally heterochromatic (15). In addition, H2B ubiquitination is necessary for sporulation (37). In yeast, ubiquitination of H2A has not been shown, and site-directed mutagenesis of the putative ubiquitination site of H2A revealed no phenotype (47). The function of histone ubiquitination in mammalian cells is unknown. The data presented in this paper show that ubi-H2A marks certain inactive chromatin regions in mammalian cells.

In the present study, we observed accumulation of ubi-H2A on the Barr body. It has been shown that a general deubiquitination of histones precedes mitosis, followed by reubiquitination in the daughter cells (28, 55). This may explain why, in the present experiments, a portion of the nuclei showed no Barr body-associated ubi-H2A accumulation. Inactivation of one of the two X chromosomes in female somatic cells during embryonic development requires a functional *Xist* locus. However, *Xist* function is not essential for inactivation of X and Y chromosomes in male meiotic prophase (50). Therefore, the mechanisms of Barr body formation and XY body formation are essentially different. Increased methylation of H3 at lysine 27 is a relatively early event in somatic X chromosome inactivation, and recruitment of the methylase requires *Xist* function (36). Here we show that XY body formation is not accompanied by H3 lysine 27 trimethylation. However, subsequent parts of the X and XY inactivation mechanisms may still overlap. For example, macroH2A1 variants are enriched in both the Barr body and the XY body (7, 17).

In the XY bodies of mouse spermatocytes, ubiquitination of H2A appears to be a relatively late event compared to accumulation of γ-H2AX. This may indicate that ubi-H2A is not involved in the formation of silent chromatin but rather is involved in maintenance of an inactive chromatin state.

We also found increased ubiquitination of H2A at silent chromatin regions of (near) telomeric sites in late pachytene and early diplotene spermatocyte nuclei. Focal sites of ubi-H2A formation in other unidentified regions of the nuclei are also apparent. ubi-H2A marks several regions of silent chromatin, although it needs to be emphasized that not all silent chromatin carries the ubi-H2A mark. It will be of interest to study the relationship between H2A ubiquitination and histone modifications other than the ones investigated here, to obtain more insight into possible roles of H2A ubiquitination in regulation of the histone code in vertebrates.

In this report we show that Hr6a/b and Rad18^{Sc}, an ubiquitin ligase that can associate with HR6a/b, colocalize with ubi-H2A in the XY bodies of meiotic cells. These results are consistent with the hypothesis that Hr6a/b may ubiquitinate H2A in the XY body, but it is not expected that Rad18^{Sc} functions as an E3 for H2A ubiquitination. In yeast, mutation of *RAD18* does not lead to defects in histone ubiquitination (46). Rather, RAD18 is though to function specifically in replicative damage bypass, a mechanism that allows replication of damaged DNA.

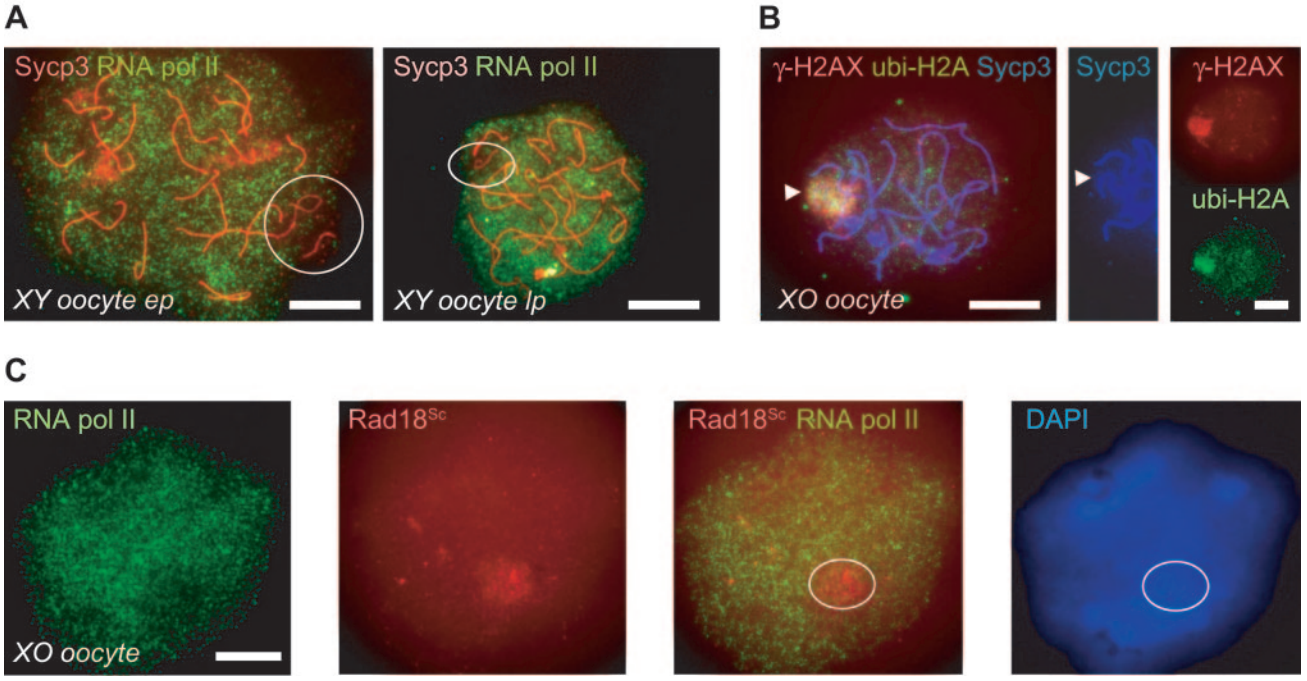

FIG. 7. Transcriptional repression of XY chromosomes in XO and XY^{tdym1} oocytes. A: Early (ep) and late (lp) pachytene XY^{tdym1} oocyte spread nuclei immunostained with anti-Sycp3 (red) and anti-RNA polymerase (pol) II (green). The area with unsynapsed synaptonemal complex axes and low RNA pol II immunoexpression is circled. B: Pachytene XO oocyte spread nucleus with accumulation of γ-H2AX (red) and ubi-H2A (green) on the unsynapsed X chromosome (arrowhead). Immunostaining of Sycp3 is shown in blue. The middle panel shows the region that contains the unsynapsed X chromosome. The panels on the right show the single γ-H2AX (red) and ubi-H2A (green) immunostainings. C: The four panels show one XO oocyte spread nucleus. RNA pol II immunoexpression (green) is relatively low in regions with intense DAPI staining (blue) and also in a $Rad18^{Sc}$-positive region (red, Rad18) that is circled in the merge and DAPI panels. Bars, 20 μm.

Based on these findings for yeast, functional involvement of $Rad18^{Sc}$ in histone ubiquitination in mouse is not expected, but formally it cannot be excluded. However, it appears more likely that Hr6a/b together with $Rad18^{Sc}$ acts to ubiquitinate an as-yet-unknown protein substrate, which might be functionally involved in maintenance of silencing of unpaired DNA, as described below.

The present findings show a reduced level of RNA polymerase II and increased accumulation of the XY body markers γ-H2AX, $Rad18^{Sc}$, and ubi-H2A on unsynapsed chromatin regions in spermatocytes and oocytes. We conclude that meiotic prophase cells are capable of detecting unpaired chromatin regions and that this activates a mechanism leading to transcriptional silencing.

MSUD in mammalian meiosis. Recent data point to the existence of a mechanism that leads to meiotic silencing by unpaired DNA (MSUD) in *Neurospora crassa* (42, 43) and *Caenorhabditis elegans* (4), which may have evolved as part of a more general genome surveillance system. During meiotic prophase, mobile or foreign DNA (transposon or virus) or translocated chromosome regions can be recognized, because these sequences will not have or find a pairing partner. The capacity of cells to detect unpaired DNA can be viewed as a means to trace and silence such DNA. For *C. elegans*, it has been shown that multiple copies of a transgene are often silenced during meiosis (20). In addition, the X chromosome of *C. elegans* males (XO) is silenced during meiotic prophase, and an epigenetic modification is maintained as an imprint during fertilization and subsequent embryo development (4, 21). It appears that MSUD has been adapted to cope with the normal presence of a single sex chromosome in male *C. elegans* meiosis.

Here we provide evidence that MSUD also occurs during male and female meiosis in mice. This sheds new light on the evolutionary origin of the XY body. During meiotic prophase, the X and Y chromosomes require specialized mechanisms to ensure that they pair and recombine, but only in the pseudoautosomal regions. We suggest that formation of the mammalian XY body, in essence, represents MSUD.

Early detailed investigations of the meiotic behavior of translocation chromosomes in mouse and human have shown that unsynapsed regions become included in the heterochromatic XY body in pachytene spermatocytes, suggesting transcriptional inactivation (see references 10 and 14 and references therein). However, such aberrant XY bodies show some residual transcriptional activity that is not present in normal XY bodies (44), which may signify that silencing of the X and Y chromosomes precedes silencing of other unpaired chromatin regions or is more effective, or both.

Since we have shown in this report that transcriptional inactivation of the 1^{13} bivalent in T/T′ mouse spermatocytes depends on the degree of asynapsis, there may be a threshold length of unpaired DNA that is required to activate MSUD. In addition, unpaired chromatin regions undergo heterologous synapsis, which appears to lead to an escape from MSUD in the male as well as the female models used here. In *N. crassa*,

MSUD occurs at the single-gene level and requires components of the RNA interference machinery (19). Barr body and XY body formation might require noncoding RNAs, derived from the *Xist* locus to initiate Barr body formation and from an unknown site for XY body formation.

The XY body and the Barr body have recently been shown to be functionally related in terms of a father-to-daughter relationship. Meiotic inactivation of the paternal X (Xp) in mouse spermatogenesis generates an epigenetic imprint that is carried on to the next generation, as evidenced by preferential inactivation of Xp in early female mouse embryos, before onset of random X inactivation (18, 26, 30). From this perspective, it will be of interest to study H2A ubiquitination during early embryonic development.

ACKNOWLEDGMENTS

We are very thankful to Paul Burgoyne and Shanti Mahadevaiah (National Institute for Medical Research, London, United Kingdom) for stimulating discussions and for making the XY^{tdym1} and XO mice available to us, to Christa Heyting (Wageningen University, Wageningen, The Netherlands) for the anti-Sycp3 antibodies, and to Mark Zijlmans (Erasmus MC, Rotterdam, The Netherlands) for the telomere probe.

This work was supported by the Dutch Science Foundation (NWO) through GB-MW (Medical Sciences) and by the Dutch Cancer Society (grant EUR 99-2003).

ADDENDUM IN PROOF

Our finding that unsynapsed chromosomal regions are transcriptionally silenced during pachytene in male and female meiosis has also recently been reported by others (J. Turner et al., Nat. Genet. 10.1038/ng1484, 5 December 2004 [Online].).

REFERENCES

1. **Baarends, W. M., J. W. Hoogerbrugge, H. P. Roest, M. Ooms, J. Vreeburg, J. H. J. Hoeijmakers, and J. A. Grootegoed.** 1999. Histone ubiquitination and chromatin remodeling in mouse spermatogenesis. Dev. Biol. **207:**322–333.
2. **Bailly, V., J. Lamb, P. Sung, S. Prakash, and L. Prakash.** 1994. Specific complex formation between yeast RAD6 and RAD18 proteins: a potential mechanism for targeting RAD6 ubiquitin-conjugating activity to DNA damage sites. Genes Dev. **8:**811–820.
3. **Barr, M. L., and E. G. Bertram.** 1949. A morphological distinction between neurones of the male and female, and the behaviour of the nucleolar satellite during accelerated nucleoprotein synthesis. Nature **163:**676–677.
4. **Bean, C. J., C. E. Schaner, and W. G. Kelly.** 2004. Meiotic pairing and imprinted X chromatin assembly in *Caenorhabditis elegans*. Nat. Genet. **36:** 100–105.
5. **Briggs, S. D., T. Xiao, Z. W. Sun, J. A. Caldwell, J. Shabanowitz, D. F. Hunt, C. D. Allis, and B. D. Strahl.** 2002. Gene silencing: trans-histone regulatory pathway in chromatin. Nature **418:**498.
6. **Chen, H. Y., J. M. Sun, Y. Zhang, J. R. Davie, and M. L. Meistrich.** 1998. Ubiquitination of histone H3 in elongating spermatids of rat testes. J. Biol. Chem. **273:**13165–13169.
7. **Costanzi, C., and J. R. Pehrson.** 1998. Histone macroH2A1 is concentrated in the inactive X chromosome of female mammals. Nature **393:**599–601.
8. **Daniel, J. A., M. S. Torok, Z. W. Sun, D. Schieltz, C. D. Allis, J. R. Yates III, and P. A. Grant.** 2004. Deubiquitination of histone H2B by a yeast acetyltransferase complex regulates transcription. J. Biol. Chem. **279:**1867–1871.
9. **Davie, J. R.** 1982. Two-dimensional gel systems for rapid histone analysis for use in minislab polyacrylamide gel electrophoresis. Anal. Biochem. **120:**276–281.
10. **de Boer, P., and A. Groen.** 1974. Fertility and meiotic behavior of male T70H tertiary trisomics of the mouse (*Mus musculus*): a case of preferential telomeric meiotic pairing in a mammal. Cytogenet. Cell Genet. **13:**489–510.
11. **de Boer, P., A. G. Searle, F. A. van der Hoeven, D. G. de Rooij, and C. V. Beechey.** 1986. Male pachytene pairing in single and double translocation heterozygotes and spermatogenic impairment in the mouse. Chromosoma **93:**326–336.
12. **Dover, J., J. Schneider, M. A. Boateng, A. Wood, K. Dean, M. Johnston, and A. Shilatifard.** 2002. Methylation of histone H3 by COMPASS requires ubiquitination of histone H2B by RAD6. J. Biol. Chem. **277:**28368–28371.
13. **Fernandez-Capetillo, O., S. K. Mahadevaiah, A. Celeste, P. J. Romanienko, R. D. Camerini-Otero, W. M. Bonner, K. Manova, P. Burgoyne, and A. Nussenzweig.** 2003. H2AX is required for chromatin remodeling and inactivation of sex chromosomes in male mouse meiosis. Dev. Cell **4:**497–508.
14. **Guichaoua, M. R., A. de Lanversin, C. Cataldo, D. Delafontaine, C. Alasia, M. Fraterno, P. Terriou, A. Stahl, and J. M. Luciani.** 1991. Three dimensional reconstruction of human pachytene spermatocyte nuclei of a 17;21 reciprocal translocation carrier: study of XY-autosome relationships. Hum. Genet. **87:**709–715.
15. **Henry, K. W., A. Wyce, W. S. Lo, L. J. Duggan, N. C. Emre, C. F. Kao, L. Pillus, A. Shilatifard, M. A. Osley, and S. L. Berger.** 2003. Transcriptional activation via sequential histone H2B ubiquitylation and deubiquitylation, mediated by SAGA-associated Ubp8. Genes Dev. **17:**2648–2663.
16. **Heyting, C.** 1996. Synaptonemal complexes: structure and function. Curr. Opin. Cell Biol. **8:**389–396.
17. **Hoyer-Fender, S., C. Costanzi, and J. R. Pehrson.** 2000. Histone macroH2A1.2 is concentrated in the XY-body by the early pachytene stage of spermatogenesis. Exp. Cell Res. **258:**254–260.
18. **Huynh, K. D., and J. T. Lee.** 2003. Inheritance of a pre-inactivated paternal X chromosome in early mouse embryos. Nature **426:**857–862.
19. **Hynes, M. J., and R. B. Todd.** 2003. Detection of unpaired DNA at meiosis results in RNA-mediated silencing. Bioessays **25:**99–103.
20. **Kelly, W. G., and A. Fire.** 1998. Chromatin silencing and the maintenance of a functional germline in *Caenorhabditis elegans*. Development **125:**2451–2456.
21. **Kelly, W. G., C. E. Schaner, A. F. Dernburg, M. H. Lee, S. K. Kim, A. M. Villeneuve, and V. Reinke.** 2002. X-chromosome silencing in the germline of *C. elegans*. Development **129:**479–492.
22. **Lammers, J. H., H. H. Offenberg, M. van Aalderen, A. C. Vink, A. J. Dietrich, and C. Heyting.** 1994. The gene encoding a major component of the lateral elements of synaptonemal complexes of the rat is related to X-linked lymphocyte-regulated genes. Mol. Cell. Biol. **14:**1137–1146.
23. **Lawrence, C.** 1994. The *RAD6* repair pathway in *Saccharomyces cerevisiae*: what does it do, and how does it do it? Bioessays **16:**253–258.
24. **Lovell-Badge, R., and E. Robertson.** 1990. XY female mice resulting from a heritable mutation in the primary testis-determining gene, *Tdy*. Development **109:**635–646.
25. **Mahadevaiah, S. K., J. M. Turner, F. Baudat, E. P. Rogakou, P. de Boer, J. Blanco-Rodriguez, M. Jasin, S. Keeney, W. M. Bonner, and P. S. Burgoyne.** 2001. Recombinational DNA double-strand breaks in mice precede synapsis. Nat. Genet. **27:**271–276.
26. **Mak, W., T. B. Nesterova, M. de Napoles, R. Appanah, S. Yamanaka, A. P. Otte, and N. Brockdorff.** 2004. Reactivation of the paternal X chromosome in early mouse embryos. Science **303:**666–669.
27. **Matsui, S., A. A. Sandberg, S. Negoro, B. K. Seon, and G. Goldstein.** 1982. Isopeptidase: a novel eukaryotic enzyme that cleaves isopeptide bonds. Proc. Natl. Acad. Sci. USA **79:**1535–1539.
28. **Matsui, S. I., B. K. Seon, and A. A. Sandberg.** 1979. Disappearance of a structural chromatin protein A24 in mitosis: implications for molecular basis of chromatin condensation. Proc. Natl. Acad. Sci. USA **76:**6386–6390.
29. **Monesi, V.** 1965. Differential rate of ribonucleic acid synthesis in the autosomes and sex chromosomes during male meiosis in the mouse. Chromosoma **17:**11–21.
30. **Okamoto, I., A. P. Otte, C. D. Allis, D. Reinberg, and E. Heard.** 2004. Epigenetic dynamics of imprinted X inactivation during early mouse development. Science **303:**644–649.
31. **Peters, A. H., S. Kubicek, K. Mechtler, R. J. O'Sullivan, A. A. Derijck, L. Perez-Burgos, A. Kohlmaier, S. Opravil, M. Tachibana, Y. Shinkai, J. H. Martens, and T. Jenuwein.** 2003. Partitioning and plasticity of repressive histone methylation states in mammalian chromatin. Mol. Cell **12:**1577–1589.
32. **Peters, A. H., A. W. Plug, and P. de Boer.** 1997. Meiosis in carriers of heteromorphic bivalents: sex differences and implications for male fertility. Chromosome Res. **5:**313–324.
33. **Peters, A. H., A. W. Plug, M. J. van Vugt, and P. de Boer.** 1997. A drying-down technique for the spreading of mammalian meiocytes from the male and female germline. Chromosome Res. **5:**66–68.
34. **Pickart, C. M.** 2004. Back to the future with ubiquitin. Cell **116:**181–190.
35. **Pickart, C. M., and R. E. Cohen.** 2004. Proteasomes and their kin: proteases in the machine age. Nat. Rev. Mol. Cell. Biol. **5:**177–187.
36. **Plath, K., J. Fang, S. K. Mlynarczyk-Evans, R. Cao, K. A. Worringer, H. Wang, C. C. de la Cruz, A. P. Otte, B. Panning, and Y. Zhang.** 2003. Role of histone H3 lysine 27 methylation in X inactivation. Science **300:**131–135.
37. **Robzyk, K., J. Recht, and M. A. Osley.** 2000. Rad6-dependent ubiquitination of histone H2B in yeast. Science **287:**501–504.
38. **Roest, H. P., W. M. Baarends, J. de Wit, J. W. van Klaveren, E. Wassenaar, J. W. Hoogerbrugge, W. A. van Cappellen, J. H. Hoeijmakers, and J. A. Grootegoed.** 2004. The ubiquitin-conjugatin DNA repair enzyme HR6A is a maternal factor essential for early embryonic development in mice. Mol. Cell. Biol. **24:**5485–5495.
39. **Roest, H. P., J. van Klaveren, J. de Wit, C. G. van Gurp, M. H. M. Koken, M. Vermey, J. H. van Roijen, J. T. M. Vreeburg, W. M. Baarends, D. Bootsma, J. A. Grootegoed, and J. H. J. Hoeijmakers.** 1996. Inactivation of

the HR6B ubiquitin-conjugating DNA repair enzyme in mice causes a defect in spermatogenesis associated with chromatin modification. Cell **86:**799–810.
40. **Rogakou, E. P., D. R. Pilch, A. H. Orr, V. S. Ivanova, and W. M. Bonner.** 1998. DNA double-stranded breaks induce histone H2AX phosphorylation on serine 139. J. Biol. Chem. **273:**5858–5868.
41. **Rougeulle, C., J. Chaumeil, K. Sarma, C. D. Allis, D. Reinberg, P. Avner, and E. Heard.** 2004. Differential histone H3 Lys-9 and Lys-27 methylation profiles on the X chromosome. Mol. Cell. Biol. **24:**5475–5484.
42. **Shiu, P. K., and R. L. Metzenberg.** 2002. Meiotic silencing by unpaired DNA: properties, regulation and suppression. Genetics **161:**1483–1495.
43. **Shiu, P. K., N. B. Raju, D. Zickler, and R. L. Metzenberg.** 2001. Meiotic silencing by unpaired DNA. Cell **107:**905–916.
44. **Speed, R. M.** 1986. Abnormal RNA synthesis in sex vesicles of tertiary trisomic male mice. Chromosoma **93:**267–270.
45. **Strahl, B. D., and C. D. Allis.** 2000. The language of covalent histone modifications. Nature **403:**41–45.
46. **Sun, Z. W., and C. D. Allis.** 2002. Ubiquitination of histone H2B regulates H3 methylation and gene silencing in yeast. Nature **418:**104–108.
47. **Swerdlow, P. S., T. Schuster, and D. Finley.** 1990. A conserved sequence in histone H2A which is a ubiquitination site in higher eucaryotes is not required for growth in *Saccharomyces cerevisiae*. Mol. Cell. Biol. **10:**4905–4911.
48. **Thiriet, C., and P. Albert.** 1995. Rapid and effective Western blotting of histones from acid-urea-Triton and sodium dodecyl sulfate polyacrylamide gels: two different approaches depending on the subsequent qualitative or quantitative analysis. Electrophoresis **16:**357–361.
49. **Turner, J. M., S. K. Mahadevaiah, R. Benavente, H. H. Offenberg, C. Heyting, and P. S. Burgoyne.** 2000. Analysis of male meiotic "sex body" proteins during XY female meiosis provides new insights into their functions. Chromosoma **109:**426–432.
50. **Turner, J. M., S. K. Mahadevaiah, D. J. Elliott, H. J. Garchon, J. R. Pehrson, R. Jaenisch, and P. S. Burgoyne.** 2002. Meiotic sex chromosome inactivation in male mice with targeted disruptions of *Xist*. J. Cell Sci. **115:**4097–4105.
51. **van der Laan, R., W. M. Baarends, E. Wassenaar, H. P. Roest, J. H. Hoeijmakers, and J. A. Grootegoed.** DNA lesion bypass proteins in spermatogenesis. Int. J. Androl., in press.
52. **van der Laan, R., H. Roest, J. Hoogerbrugge, E. Smit, R. Slater, W. Baarends, J. Hoeijmakers, and J. Grootegoed.** 2000. Characterization of mRAD18Sc, a mouse homolog of the yeast post-replication repair gene RAD18. Genomics **69:**86–94.
53. **van der Laan, R., E.-J. Uringa, E. Wassenaar, J. W. Hoogerbrugge, E. Sleddens, H. Odijk, H. P. Roest, P. de Boer, J. H. Hoeijmakers, J. A. Grootegoed, and W. M. Baarends.** 2004. Ubiquitin ligase Rad18Sc localizes to the XY body and to other chromosomal regions that are unpaired and transcriptionally silenced during male meiotic prophase. J. Cell Sci. **117:**5023–5033.
54. **Vassilev, A. P., H. H. Rasmussen, E. I. Christensen, S. Nielsen, and J. E. Celis.** 1995. The levels of ubiquitinated histone H2A are highly upregulated in transformed human cells: partial colocalization of uH2A clusters and PCNA/cyclin foci in a fraction of cells in S-phase. J. Cell Sci. **108:**1205–1215.
55. **Wu, R. S., K. W. Kohn, and W. M. Bonner.** 1981. Metabolism of ubiquitinated histones. J. Biol. Chem. **256:**5916–5920.
56. **Zhang, Y.** 2003. Transcriptional regulation by histone ubiquitination and deubiquitination. Genes Dev. **17:**2733–2740.